Spatial organization of translation and translational repression in two phases of germ granules

Anne Ramat†*, Ali Haidar†, Céline Garret, Martine Simonelig*

*Corresponding authors: Martine.Simonelig@igh.cnrs.fr; Anne.Ramat@igh.cnrs.fr

Supplementary Information
The PDF file includes:

Supplementary Figures 1 to 9
Supplementary Note
Supplementary Tables 1 to 5

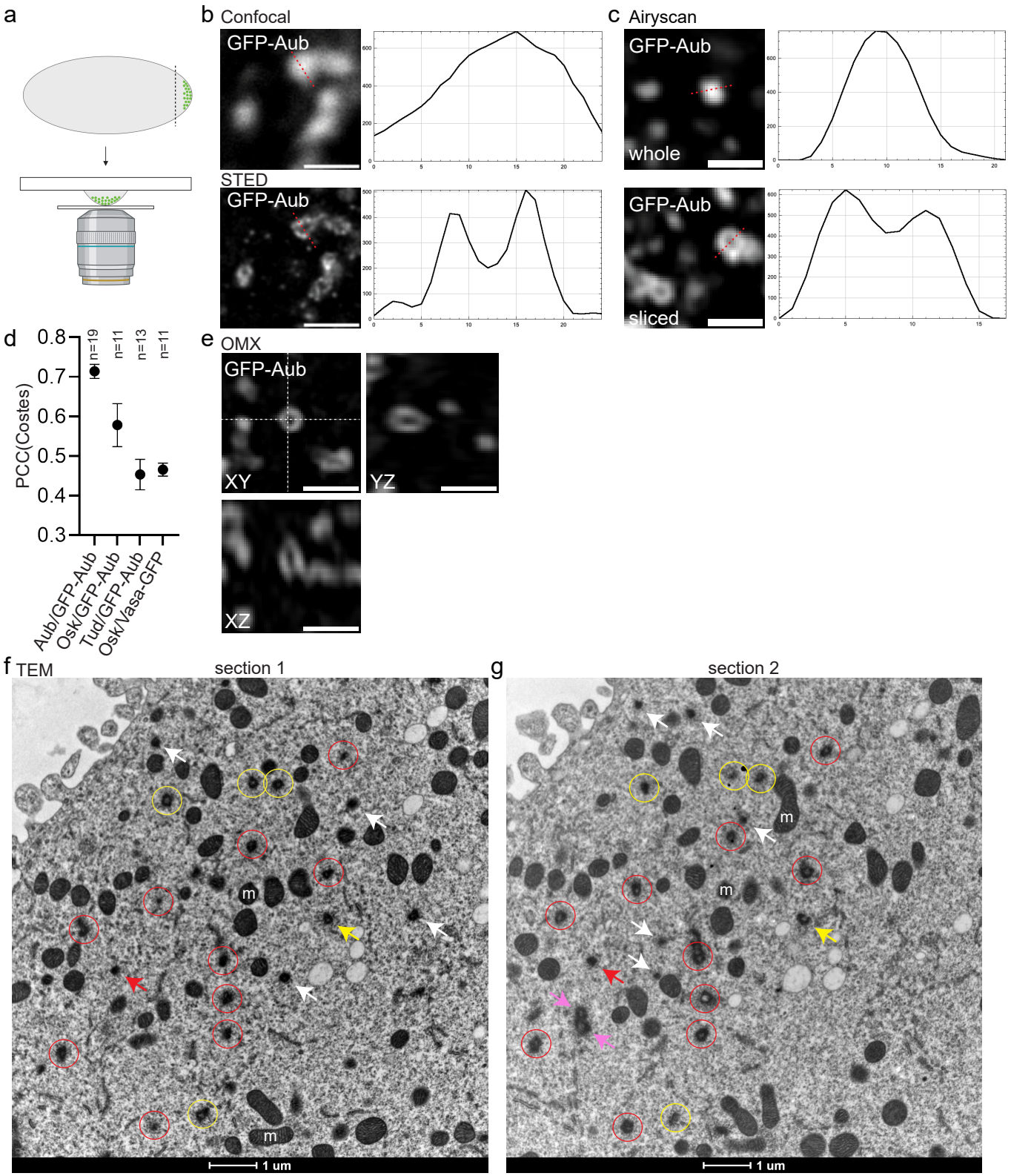

Supplementary Figure 1/ Biphasic organization of *Drosophila* germ granules visualized with three super-resolution microscopy techniques. a, Illustration of the mounting of the embryo posterior following slicing. Created with BioRender.com **b**, Immunostaining of *UASp-GFP-Aub; nos-Gal4* embryos with anti-GFP antibody, showing the same germ granules imaged using confocal (top) or STED super-resolution (bottom) microscopy. Fluorescence intensity (right) was recorded along the path marked with a red line. **c**, Airyscan imaging of *UASp-GFP-Aub; nos-Gal4* embryos in whole mount (top) or as a sliced posterior pole (bottom). Fluorescence intensity (right) was recorded along the path marked with a red line. GFP fluorescence was directly recorded without antibody staining. **d**, Quantification of colocalization between the indicated components shown in Fig. 1a, using PCC(Costes). Black circles represent the mean and error bars represent SEM. The number of embryos is indicated (n). **e**, 3D-OMX imaging of an *UASp-GFP-Aub; nos-Gal4* sliced posterior pole. YZ and XZ show the orthogonal views of the acquisition. GFP fluorescence was directly recorded without antibody staining. **f, g**, Electron micrographs of consecutive ultra-thin sections of the same germ plasm. Yellow circles indicate germ granules that are hollow in section 1 and full in section 2. Red circles indicate germ granules that are full in section 1 and hollow in section 2. The red arrow indicates a germ granule full in both sections. The yellow arrow indicates a germ granule hollow in both sections. White arrows indicate full germ granules present in one section only. Pink arrows indicate hollow germ granules present in one section only. m indicate examples of mitochondria. Scale bars: 1 µm. Source data are provided as a Source Data file.

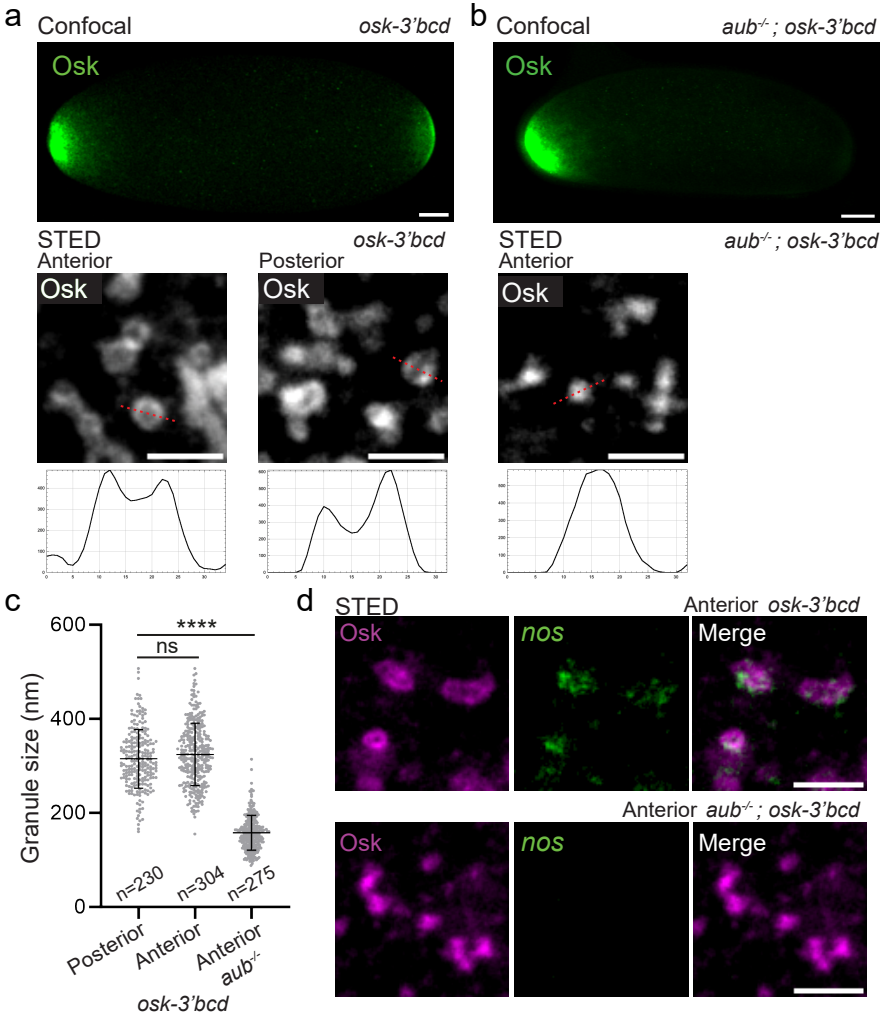

Supplementary Figure 2/ Defective germ granule organization in the absence of Aub. a, Immunostaining of *UASp-osk-bcd3'UTR/nos-Gal4* (*osk-3'bcd*) embryos with anti-Osk antibody showing Osk protein localization at both poles using confocal microscopy (top). *osk-bcd3'UTR* chimeric mRNA is recruited to the embryo anterior pole due to the presence of *bicoid* (*bcd*) 3'UTR. Visualization of germ granule organization using STED microscopy (bottom) showing that both anterior and posterior germ granules are biphasic. Fluorescence intensity was recorded along the path marked with a red dotted line. **b**, Immunostaining of *aub*$^{QC42/HN2}$*; UASp-osk-bcd3'UTR/nos-Gal4* (*aub*$^{-/-}$*; osk-3'bcd*) embryos with anti-Osk antibody showing Osk protein localization only at the anterior pole using confocal microscopy (top). Visualization of germ granule organization using STED microscopy (bottom) showing the loss of germ granule biphasic structure. Fluorescence intensity was recorded along the path marked with a red dotted line. **c**, Quantification of germ granule size in *UASp-osk-bcd3'UTR/nos-Gal4* (*osk-3'bcd* Posterior and Anterior) and *aub*$^{QC42/HN2}$*; UASp-osk-bcd3'UTR/nos-Gal4* (Anterior *aub*$^{-/-}$) embryos. Horizontal bars represent the mean and SD. ns: non-significant, **** p<0.0001 using the unpaired two-tailed Student's t-test. p=0.1 between anterior and posterior granules in *osk-3'bcd* embryos; p=2.9x10^{-137} between posterior granules in *osk-3'bcd* embryos and anterior granules in *aub*$^{-/-}$*; osk-3'bcd* embryos; p=1.2x10^{-153} between anterior granules in *osk-3'bcd* embryos and anterior granules in *aub*$^{-/-}$*; osk-3'bcd* embryos. The number of granules is indicated (n). **d**, STED imaging of immuno-sm-FISH of *UASp-osk-bcd3'UTR/nos-Gal4* (*osk-3'bcd*) and *aub*$^{QC42/HN2}$*; UASp-osk-bcd3'UTR/nos-Gal4* (*aub*$^{-/-}$*; osk-3'bcd*) embryos with anti-Osk antibody (magenta) and *nos* smFISH probe (green) showing the lack of *nos* mRNA in germ granules from *aub*$^{QC42/HN2}$ mutant embryos. Scale bars: 50 µm in (**a**, **b**, top), 1 µm in (**a**, **b**, bottom and **d**). Source data are provided as a Source Data file.

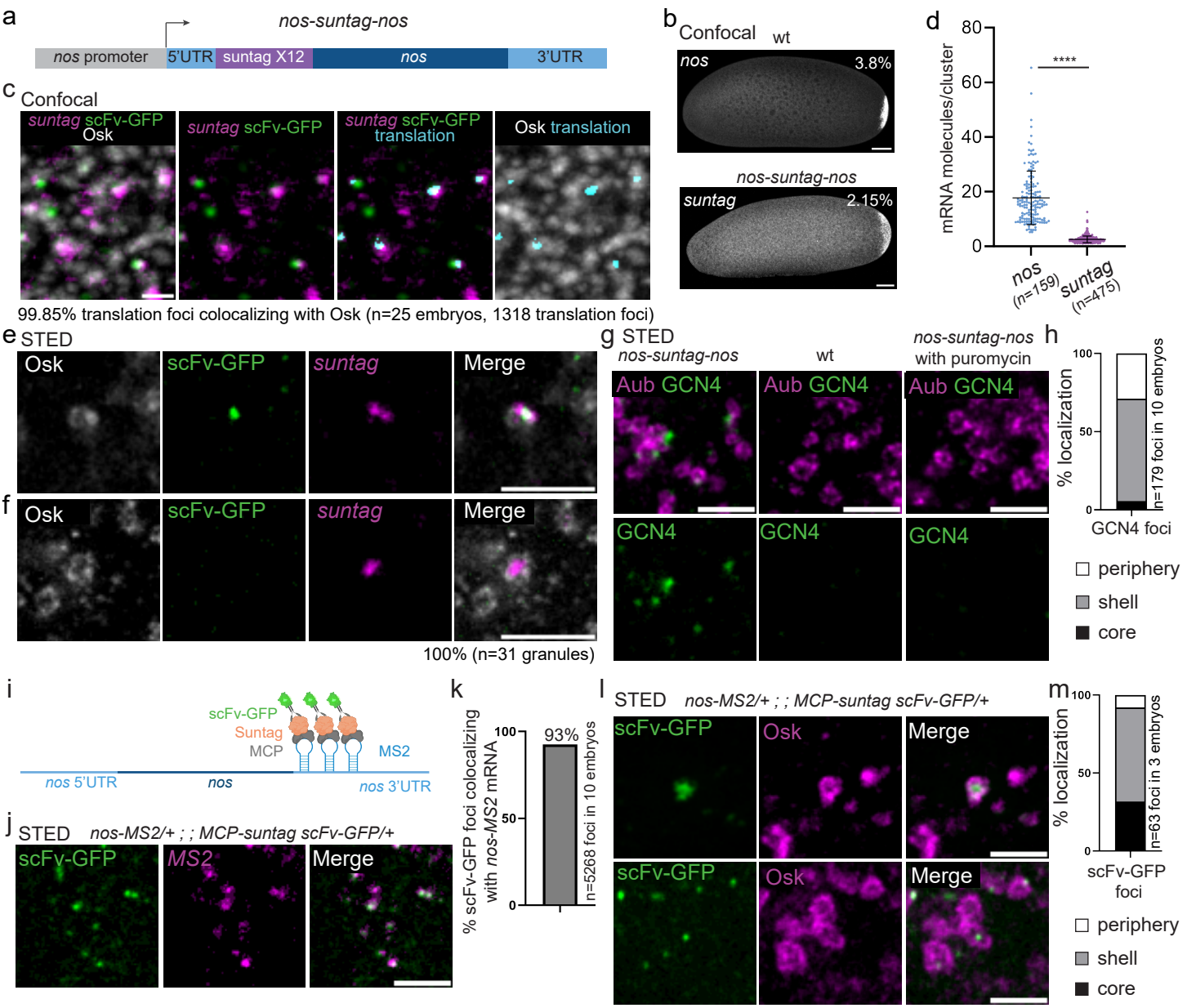

Supplementary Figure 3/ Visualization of *nos* translation at germ granules using *suntag-nos*. **a**, Schematic representation of the *nos-suntag-nos* construct. **b**, Z-projection of confocal images of smFISH on wild-type (top) and *suntag-nos/+* (bottom) embryos hybridized with *nos* and *suntag* probes, respectively. The corrected total fluorescence intensity at the posterior pole and in the whole embryo was measured to assess the percentage of mRNA localized at the posterior pole. **c**, Immuno-smFISH of *nos-suntag-nos/+; nos-scFv-GFP/+* embryos with anti-Osk antibody (grey), anti-GFP (green) nanobody to reveal scFv-GFP, and smFISH *suntag* probes (magenta). Colocalization of *suntag* and scFv-GFP signals (cyan) indicates ongoing *suntag-nos* translation. **d**, Quantification using FISH-quant of the number of *nos* and *suntag-nos* mRNA molecules per cluster at the posterior pole from confocal images of smFISH on wild-type and *nos-suntag-nos* embryos, respectively. Horizontal bars represent the mean and SD. **** p<0.0001 using the unpaired two-tailed Student's t-test. p=2.1x10^{-139}. The number of mRNA clusters is indicated (n). **e**, **f**, Three-color STED imaging of immuno-smFISH of *nos-suntag-nos/+; nos-scFv-GFP/+* embryos with anti-Osk antibody (grey), anti-GFP nanobody (green) to reveal scFv-GFP and smFISH *suntag* probes (magenta). **g**, STED imaging of *nos-suntag-nos/+* (left), wild-type (middle) and *nos-suntag-nos/+* treated with puromycin (right) embryos immunostained with anti-Aub (magenta) and anti-GCN4 (green) antibodies. **h**, Percentage of GCN4 foci localized in the core (black), in the shell (grey) and at the immediate periphery (white) of germ granules from images of *nos-suntag-nos/+* embryos as shown in (**g**). **i**, Illustration of the *nos-MS2*/MCP-Suntag system to localize scFv-GFP to the core of germ granule. Created with BioRender.com (**j**) Immuno-smFISH of *nos-MS2/+; nos-MCP-suntag nos-scFv-GFP/+* embryos with anti-GFP (green) to reveal scFv-GFP and smFISH *MS2* probes (magenta). **k,** Percentage of scFv-GFP foci colocalizing with *nos-MS2* mRNA obtained from images as in (**j**). (**l**) STED imaging of *nos-MS2/+; nos-MCP-suntag nos-scFv-GFP/+* embryos immunostained with anti-Osk antibody (magenta) and anti-GFP nanobody (green) to reveal scFv-GFP. (**m**) Percentage of scFv-GFP foci localized in the core (black), in the shell (grey) and at the immediate periphery (white) of germ granules obtained from images as shown in (**l**). Scale bars: 50 µm in (**b**), 1 µm in (**c**, **e**, **f**, **g**, **j, l**). Source data are provided as a Source Data file.

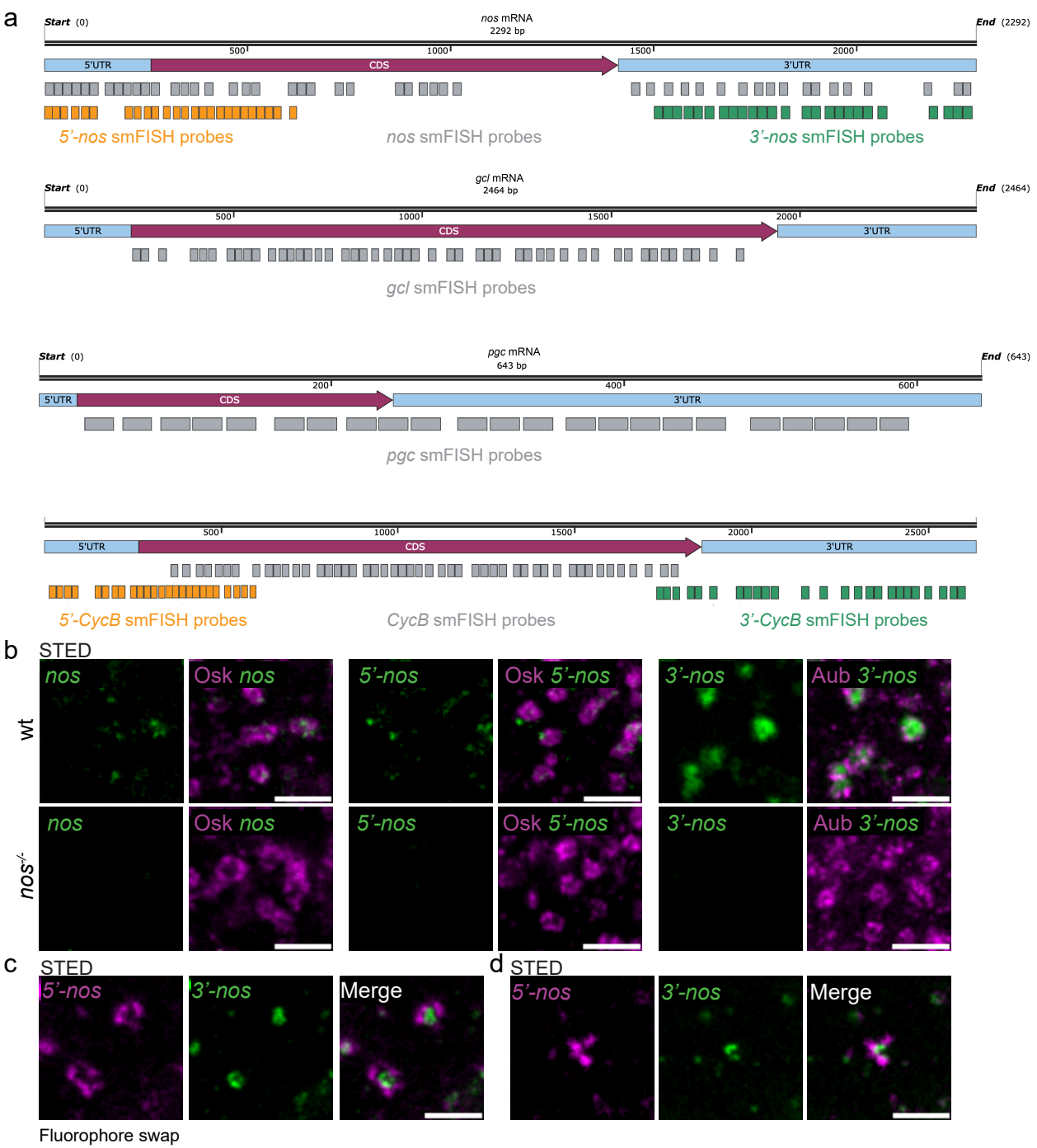

Supplementary Figure 4/ Schematic representation and validation of smFISH probes. a, The boxes represent oligos composing the probes. Grey boxes indicate probes covering full length mRNAs or coding sequences; orange boxes indicate probes covering mRNA 5'ends; and green boxes indicate probes covering mRNA 3'ends. **b**, STED imaging of immuno-smFISH of wild-type (top) and *nos*^{BN} (bottom) embryos with anti-Osk or anti-Aub antibodies (magenta) and *nos*, *5'-nos* or *3'-nos* smFISH probes (green) showing the lack of signals with each *nos* probe in *nos*^{BN} mutant embryos. **c**, **d**, STED images of smFISH of wild-type embryos with *5'-nos* (magenta) and *3'-nos* (green) probes where fluorophores associated with the probes have been swapped compared to images shown in Fig. 5a. Example of a granule in which three *nos* mRNA molecules are visible with both the *5'-nos* and *3'-nos* probes (**d**). Scale bars: 1 µm.

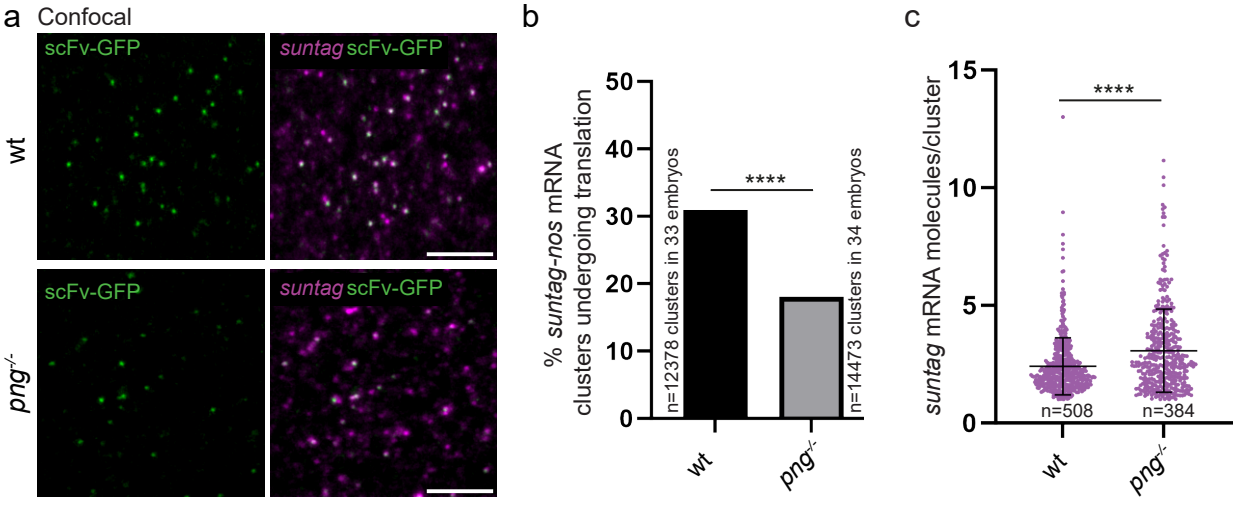

Supplementary Figure 5/ Decrease of translation in *png* mutant embryos. a, Fluorescent confocal imaging of smFISH on *nos-suntag-nos/+; nos-scFv-GFP/+* (wt) and *png*^{1058}*; nos-suntag-nos /+; nos-scFv-GFP/+* (*png*$^{-/-}$) embryos, showing scFv-GFP (green) and *suntag-nos* mRNA (magenta). **b**, Percentage of *suntag-nos* mRNA clusters undergoing translation in *nos-suntag-nos/+; nos-scFv-GFP/+* (wt) and *png*^{1058}*; nos-suntag-nos /+; nos-scFv-GFP/+* (*png*$^{-/-}$) embryos. The graph represents the percentage of *suntag-nos* mRNA clusters colocalizing with scFv-GFP foci from images as in (**a**). **** p<0.0001 using the χ^2 test. p=1.6x10^{-133}. **c**, Quantification using FISH-quant of the number of *suntag-nos* mRNA molecules per cluster at the posterior pole from confocal images of smFISH on *nos-suntag-nos/+; nos-scFv-GFP/+* (wt) and *png*^{1058}*; nos-suntag-nos /+; nos-scFv-GFP/+* (*png*$^{-/-}$) embryos as shown in (**a**). Horizontal bars represent the mean and SD. **** p<0.0001 using the unpaired two-tailed Student's t-test. p=4.2x10^{-11}. The number of mRNA clusters is indicated (n). Scale bars: 5 µm. Source data are provided as a Source Data file.

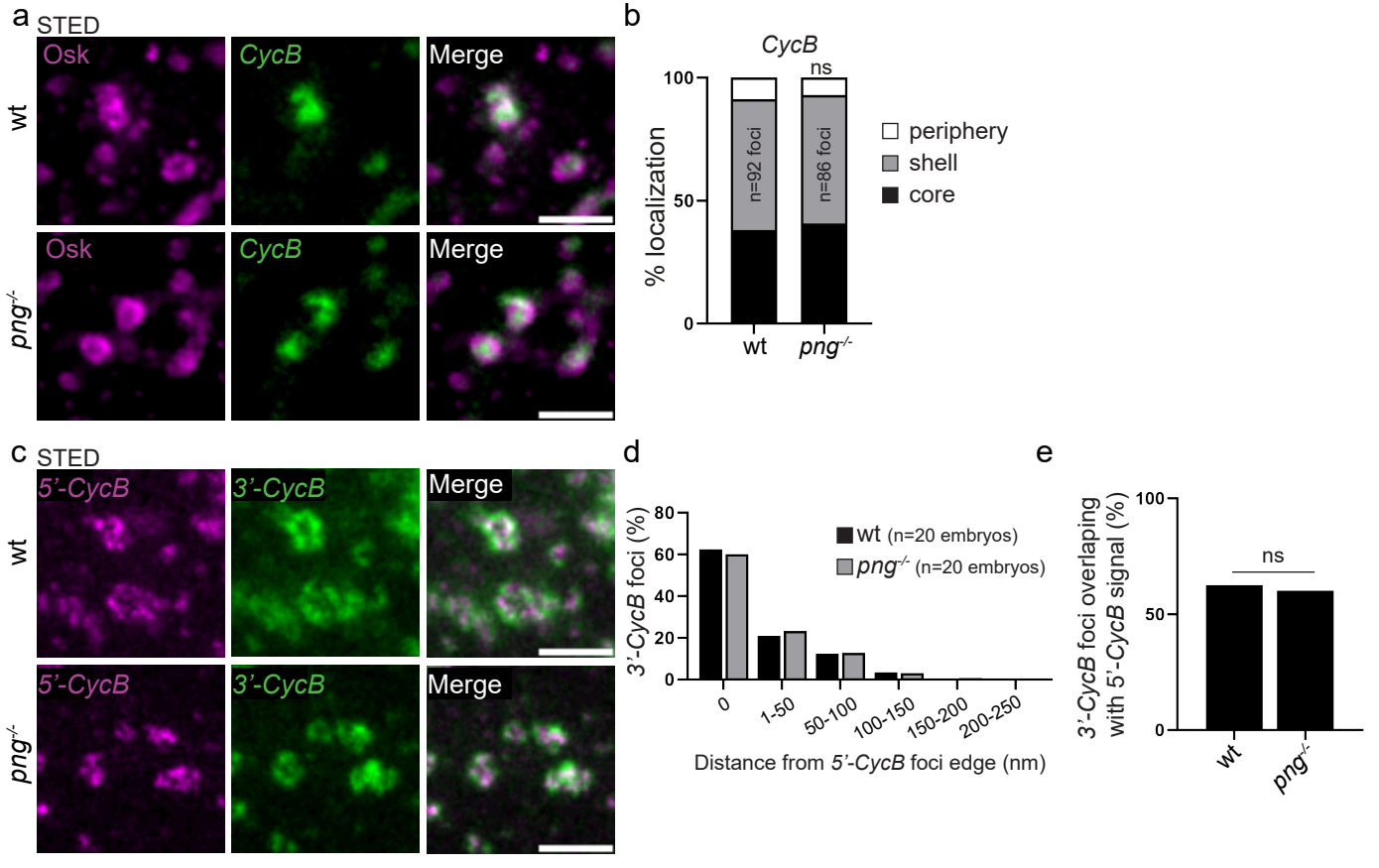

Supplementary Figure 6/ *CycB* mRNA localization and compaction are not affected in *png* mutant embryos. **a**, STED imaging of immuno-smFISH of wild-type and *png*^{1058} mutant (*png*$^{-/-}$) embryos with anti-Osk antibody and *CycB* smFISH probe. **b**, Percentage of localization of *CycB* mRNA foci in wild-type and *png*^{1058} mutant embryos, in the core (black), in the shell (grey) and at the immediate periphery (white) of germ granules from images as in (**a**). ns: non-significant using the χ^2 test. p=0.88. **c**, STED images of smFISH against *CycB* 5'end (*5'-CycB*, magenta) and 3'end (*3'-CycB*, green) in wild-type and *png*^{1058} mutant embryos. **d**, Measurement of the distance between *CycB* 3'end foci and the edge of *CycB* 5'end foci in wild-type and *png*^{1058} embryos from images as in (**c**). The histogram shows the percentage of *CycB* 3'end foci in each distance class. **e**, Percentage of *CycB* 3'end foci overlaping with *CycB* 5'end foci in wild-type and *png*^{1058} embryos. ns: non-significant using the χ^2 test. p=0.09. Scale bars: 1 µm. Source data are provided as a Source Data file.

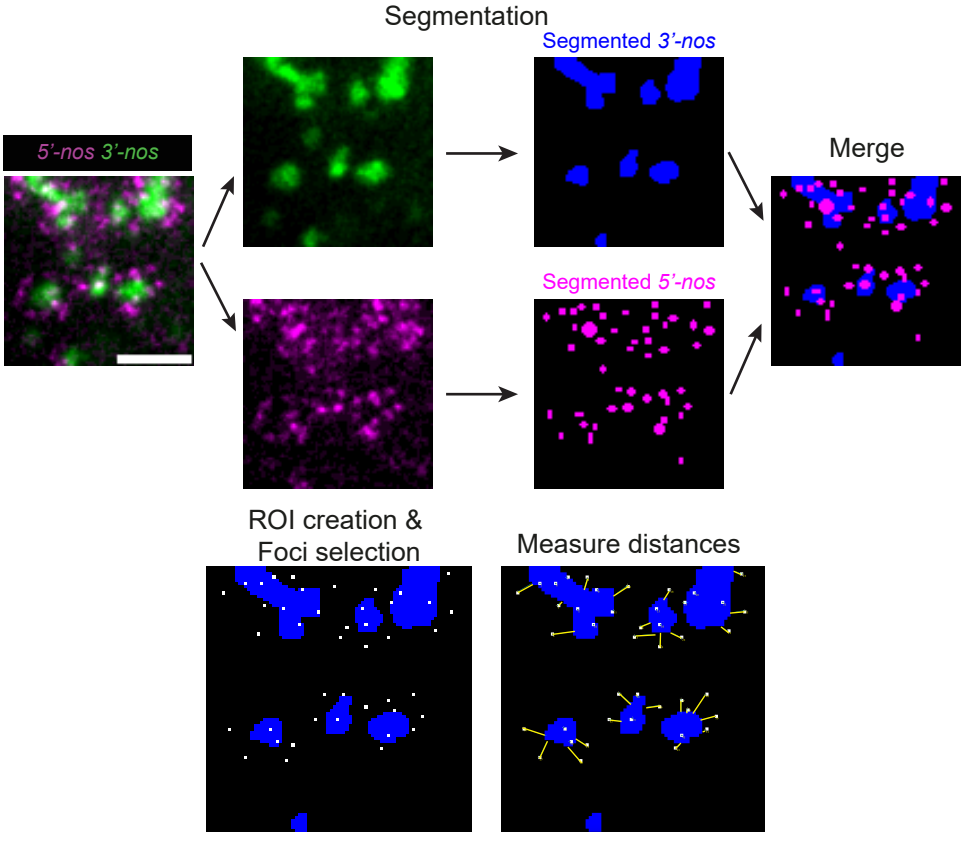

Supplementary Figure 7/ Illustration of the method to measure the distance between 5'end and 3'end smFISH probes. The most internal signal, here *3'-nos* in green, was segmented to define regions of interest (ROI) that corresponded to the area of the probe signal. The signal from *5'-nos* smFISH probes in magenta was segmented as foci. The distance between the edge of the ROI defined by *3'-nos* and the center of *5'-nos* foci was then measured. When *5'-nos* foci were within *3'-nos* ROI, the measured distance was 0 (overlaping foci).

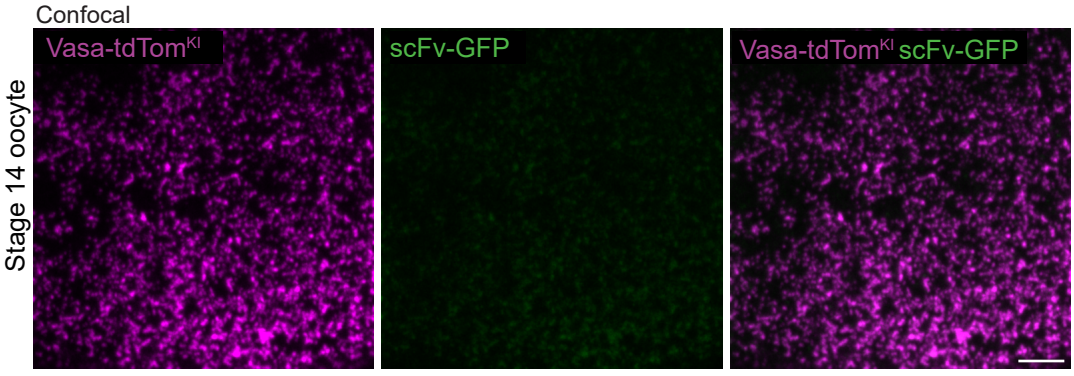

Supplementary Figure 8/ *suntag-nos* is not translated in stage 14 oocytes. Confocal image of *vasa-tdTom-^{KI}/nos-suntag-nos; nos-scFv-GFP/+* stage 14 oocyte germ plasm. GFP and tdTomato were recorded without antibody staining. The GFP fluorescence was absent in 100% of stage 14 oocytes (n=14). Scale bar: 5 µm.

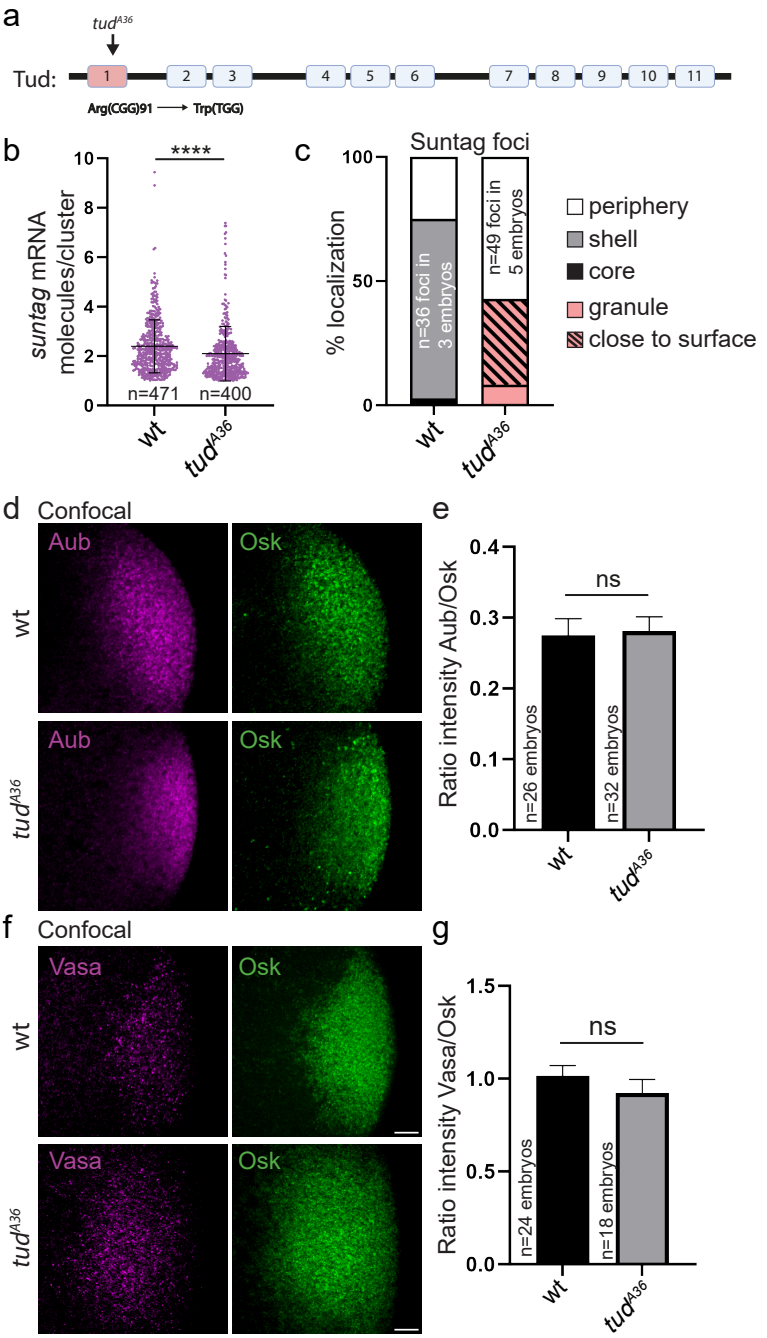

Supplementary Figure 9/ Characterization of germ granule content in *tud*^{A36} mutant. a, Schematic representation of Tud protein and the point mutation in *tud*^{A36} mutant. Boxes represent the eleven Tudor domains. The mutation in *tud*^{A36} is in the first Tudor domain. **b**, Quantification using FISH-quant of the number of *suntag-nos* mRNA molecules per cluster at the posterior pole from confocal images of smFISH on *nos-suntag-nos/+; nos-scFv-GFP/+* (wt) and *nos-suntag-nos tud*^{A36}*/Df(2R)Pu*^{rP133}*; nos-scFv-GFP/+* (*tud*^{A36}) embryos from images as in Fig. 7c. Horizontal bars represent the mean and SD. **** p<0.0001 using the unpaired two-tailed Student's t-test. p=4.4x10^{-5}. The number of mRNA clusters is indicated (n). **c**, Percentage of scFv-GFP foci in *nos-suntag-nos/+; nos-scFv-GFP/+* (wild-type) and *nos-suntag-nos tud*^{A36}*/Df(2R)Pu*^{rP133}*; nos-scFv-GFP/+* (*tud*^{A36}) embryos, localized in the core (black), the shell (grey) and at the immediate periphery (white) of wild-type germ granules, and in the monophasic germ granule (pink) and at their immediate periphery (white) in *tud*^{A36} embryos. The striped pink rectangle represents the percentage of scFv-GFP foci within 50 nm of the granule surface. **d**, Confocal images of immunostaining of wild-type (wt) and *tud*^{A36}*/Df(2R)Pu*^{rP133} (*tud*^{A36}) embryos with anti-Aub (magenta) and anti-Osk (green) antibodies. **e**, Quantification of Aub protein levels (signal intensity) normalized to Osk levels. ns: non-significant using the unpaired two-tailed Student's t-test. p=0.85. **f**, Confocal images of immunostaining of wild-type (wt) and *tud*^{A36}*/Df(2R)Pu*^{rP133} (*tud*^{A36}) embryos with anti-Vasa (magenta) and anti-Osk (green) antibodies. **g**, Quantification of Vasa protein levels (signal intensity) normalized to Osk levels. ns: non-significant using the unpaired two-tailed Student's t-test. p=0.32. Scale bars: 10 µm. Source data are provided as a Source Data file.

Supplementary Note

Imaging germ granule core/shell organization

Drosophila embryos have an ovoid shape and the germ plasm is only accessible by imaging deep into the sample, which decreases resolution. Therefore, to reach the resolution required to resolve germ granule organization, the distance between the sample and the objective had to be reduced. This was achieved using two approaches: 1) either optimizing the mounting of embryos such that the posterior pole was directly facing the coverslip, or 2) slicing the posterior of embryos. In the first approach, embryos were mounted in a high concentration, making embryos pile up one upon another. Only embryos with the posterior pole facing up were imaged. In the second approach, the posterior of embryos was sliced using a needle and mounted with the posterior side up (Extended Data Fig. 1a). Both approaches led to a level of resolution allowing to reveal germ granule structure. The requirement of these mounting methods was illustrated by imaging germ granule using the Airyscan system. This is a confocal laser scanning set up where an array of detectors allows the improvement of resolution up to 120 nm, giving super-resolution-like images. Using whole mount embryos, we could not observe germ granule core/shell organization (Extended Data Fig. 1c, top). However, using sliced posterior poles, we easily observed GFP-Aub donut-like shapes, even with GFP fluorescence, in the absence of antibody staining (Extended Data Fig. 1c, bottom). The germ granule core/shell architecture was observed using three different microscopy techniques, STED, Airyscan and OMX, with and without antibody staining, establishing this biphasic organization.

Supplementary Table 1. List of smFISH probes to detect the *suntag* sequence

Probe sequence	Probe Name
ggtggtagttcttgctcag	suntag_1
ctacccttcttcagtctgg	suntag_2
gctcaaaagttcttcaccg	suntag_3
gccacttcgttctcaagat	suntag_4
gccagaacctttcttaaga	suntag_5
tgaaagcagttcttctcca	suntag_6
tcattttccaggtggtaat	suntag_7
ccctttttcagtctagcta	suntag_8
atttttgctcagcaactcc	suntag_9
tgctacttcgttctccaaa	suntag_10
atccggacccttttctttag	suntag_11
tcgagagtaactcctcacc	suntag_12
gccacttcgttttcgagat	suntag_13
accactgccctttttagc	suntag_14
agataatagctcttctcca	suntag_15
attttcgaggtggtagttt	suntag_16
ctttttaagcgtgccacc	suntag_17
accactgccactagtactt	suntag_18
attcttggatagtagctct	suntag_19
gctacctcgttctcaagat	suntag_20
ccggaacccttcttcaaac	suntag_21
agttcttcgagagcagttc	suntag_22
gcgacctcattttcaagat	suntag_23
cccgatccctttttaatc	suntag_24
gaaagtagttcctcaccac	suntag_25
cttcgttttcgaggtggta	suntag_26
ccctgaacctttctttaat	suntag_27
actcagtaattcttcaccc	suntag_28
gctacctcattttccagat	suntag_29
aaccactcccctttttag	suntag_30
ttcgatagcaattcctcgc	suntag_31
agcaacttcgttctcaaga	suntag_32
taccagagccctttttgag	suntag_33
tacttagtaattcctcacc	suntag_34
cttgctacttcattctcta	suntag_35
gagcctgagccctttttta	suntag_36

Supplementary Table 2. List of smFISH probes to detect *nos* 5'end (*5'-nos*)

Probe sequence	Probe Name
aagctacgcgccaactaa	5'-nos_1
ttccaggaattttgtggt	5'-nos_2
aactgcgaagcgtacggc	5'-nos_3
tcgtatgtcccttagaca	5'-nos_4
aatcgtgacgcagaggca	5'-nos_5
ctaaactcgcttttgggt	5'-nos_6
ccacaaatcctcacccaa	5'-nos_7
ggttatcgcgcactctac	5'-nos_8
ggcgaaaatccgggtcga	5'-nos_9
ccaagttgctgcggaaca	5'-nos_10
aagttatctgctgctgcg	5'-nos_11
cctcctctggcgtgaaaa	5'-nos_12
tgcaggcccagaatgttg	5'-nos_13
cccactggtatccaaata	5'-nos_14
aagtggccgacgagttgg	5'-nos_15
ggcgtaatgggcggactc	5'-nos_16
agacgtcgacgggtcagg	5'-nos_17
ggaagtgcgtcgactgcg	5'-nos_18
gcgctgtcggccagaaaa	5'-nos_19
ggagcgaattggcggtgg	5'-nos_20
tggtactgtcgctgcata	5'-nos_21
tgctggagcagcaagtgg	5'-nos_22
catggccagttgctgctg	5'-nos_23
cagcgccaattggtgctg	5'-nos_24
tttgctggtgactcgcac	5'-nos_25

Supplementary Table 3. List of smFISH probes to detect *nos* 3'end (*3'-nos*)

Probe sequence	Probe Name
tctatctatctggttaacccag	3'-nos_1
caggcgctatttaaacgttact	3'-nos_2
aatctctttaaaatcgaacgcg	3'-nos_3
aagatctataggcacgggataa	3'-nos_4
tgatcgttcgttgtctatacta	3'-nos_5
ttcttgaattattgacttggat	3'-nos_6
caaaattagtttccctttcaca	3'-nos_7
acgatattgtaagtcttcttta	3'-nos_8
gccacgacgattgaacaagtat	3'-nos_9
ttcggattgtaagatatttcta	3'-nos_10
cagaccaattccattcatcaac	3'-nos_11
tttacgaaatgaaggcgaccag	3'-nos_12
atatatcgaaatttttcggccg	3'-nos_13
attcaaagtgttccttttcaa	3'-nos_14
aatgatacgattgacagttcga	3'-nos_15
tcctttagcaagatttaaattt	3'-nos_16
cgacgaaagtgttccttgctat	3'-nos_17
attttacaatgaatgcgtagcc	3'-nos_18
agtgcggaatgtcaaaatttaa	3'-nos_19
atactcttcgcttatctatcaa	3'-nos_20
gtgttgaaatgaatacttgcga	3'-nos_21
aattatataatgctggcggttg	3'-nos_22
tcagaatatgtgtacacatttt	3'-nos_23
tcgagccattgaatttttcatt	3'-nos_24
tgtaaccatttctttatttggc	3'-nos_25

Supplementary Table 4. List of smFISH probes to detect *cycB* 5'end (*5'-cycB*)

Probe sequence	Probe name
gctgccgtttgaatttga	5'-cycB_1
ttgcacacgaagcgaggc	5'-cycB_2
ctccgaaaacctgatcga	5'-cycB_3
tcgagtgcgggattgtca	5'-cycB_4
cgcttgtttagctgttga	5'-cycB_5
gatcgcgtttctgtgacc	5'-cycB_6
ggctatcacttggtttgg	5'-cycB_7
cgaagataggcagacgct	5'-cycB_8
tgcttcttttctatctgt	5'-cycB_9
ttgtgcccaccattttga	5'-cycB_10
atcgccacgcattttcag	5'-cycB_11
agttctccgaagcgttct	5'-cycB_12
tcttcaattgcacttgct	5'-cycB_13
ccatggaaggaaccgtca	5'-cycB_14
gcgcgttttgttgttgcc	5'-cycB_15
ctgcaaatcgcccaaggc	5'-cycB_16
gacgacttatgccgcgat	5'-cycB_17
gcatccttcgctgcgatg	5'-cycB_18
ccttggagtctttctgtg	5'-cycB_19
gcgtctgtgagcttgaga	5'-cycB_20
agctttggcattgcgcag	5'-cycB_21
agtggctgtttcttccag	5'-cycB_22
cattgccattgccattgg	5'-cycB_23
ttgaccttgggcggaacg	5'-cycB_24
aaaaacgccgacacgccc	5'-cycB_25

Supplementary Table 5. List of smFISH probes to detect *cycB* 3'end (*3'-cycB*)

Probe sequence	Probe name
ttcagcttggcctgaggag	3'-cycB_1
ggtacttgttgtagatggc	3'-cycB_2
gcgatcttctggaacttgc	3'-cycB_3
acaatcgagtccatcagcg	3'-cycB_4
tatttcctctggctctggc	3'-cycB_5
aaactaggtaagtcagggtct	3'-cycB_6
cgcatttttttaacgaacacga	3'-cycB_7
gcaatgcgactacggtaacta	3'-cycB_8
atgggtgatgcaggtaaagat	3'-cycB_9
ccagcagattacgatatctta	3'-cycB_10
agtagccgaaaactgctcaag	3'-cycB_11
tagtcttaccggaggaactca	3'-cycB_12
gagatggtgacccagcgaaag	3'-cycB_13
aaatgaactcgttgcccactc	3'-cycB_14
aattcttggagagacaacgcc	3'-cycB_15
tgaaatgatttcacgggtaca	3'-cycB_16
attagtgataggtaggtaggg	3'-cycB_17
tattcattcccatcgaaacta	3'-cycB_18
attttgcacaatttttggat	3'-cycB_19
ttttatgcgatttatgggaat	3'-cycB_20
ttacaaatagtctacgtctct	3'-cycB_21
tgtttttgtatgaatgtgcga	3'-cycB_22
ttttaatcgttgcttagtggt	3'-cycB_23
tttgggaaacatcagttagtt	3'-cycB_24
tctatgtattgttcagagaca	3'-cycB_25